This is a peer-reviewed, author's accepted manuscript of the following research article: Stillings, M., Shipton, Z. K., & Lunn, R. J. (Accepted/In press). Mechanochemical processing of silicate rocks to trap CO_2. *Nature Sustainability*.

Mechanochemical processing of silicate rocks to trap CO_2

Dr Mark Stillings[1], Prof. Zoe K. Shipton[1], Prof. Rebecca J. Lunn[1]*
[1] Department of Civil and Environmental Engineering, University of Strathclyde; Glasgow, UK.
**Corresponding author*
***Email:** mark.stillings@strath.ac.uk*

Abstract

Milling minerals rich in magnesium and iron within CO_2 gas has been proposed to capture carbon as metal-carbonates. We conduct milling experiments in CO_2 and show that polymineralic rocks such as granite and basalt, whether high or low in carbonate-forming metals, are more efficient at trapping CO_2 than individual minerals. This is because the trapping process is not, as previously thought, based on the carbonation of carbonate-forming metals. Instead, CO_2 is chemically adsorbed into the crystal structure, predominantly at the boundaries between different minerals. Leaching experiments on the milled mineral/rock powders show that CO_2 trapped in single minerals is mainly soluble, whereas CO_2 trapped in polymineralic rocks is not. Under ambient temperature conditions, polymineralic rocks can capture >13.4 $mgCO_2/g$ as thermally stable, insoluble CO_2. Polymineralic rocks are crushed worldwide to produce construction aggregate. If crushing processes could be conducted within a stream of effluent CO_2 gas (as produced from cement manufacture) our findings suggest that for every 100 Mt of hard rock aggregate sold, 0.4-0.5 $MtCO_2$ could be captured as a by-product.

Main

The development of increasingly efficient technologies for the capture of carbon dioxide (CO_2) emissions is key to achieving global carbon targets. Ex-situ direct mineral carbonation technologies aim to trap CO_2 in the form of carbonates. Most research has produced direct carbonation by reaction of CO_2 at elevated temperatures 400-600°C (*1-6*) with the mineral olivine (*3-4*) or with rocks rich in magnesium and calcium (carbonate-forming metals) such as dolerite, basalt and peridotite (*3-6*). The process requires significant energy input; samples must first be powdered to create a large surface area, and then reacted with CO_2 at temperatures 500°C producing trapping efficiencies of 0.255-0.26 $mgCO_2/g$ for olivine minerals (forsterite) and, 1.26-13.43 $mgCO_2/g$ for magnesium- and calcium-rich rocks such as olivine basalts, dunites, and doleritic mine waste (*3-6*).

Mechanochemistry is a branch of chemistry whereby some, or all, of the energy required for a chemical reaction is provided by the deformation of a solid substance, in this case grinding of rocks and minerals, with the aim of reducing the external energy input to the process by reducing the heat or pressure increase required *(7)*. In mechanochemistry, fracturing of the chemical bonds in solids releases charged particles and photons *(8)* and is thought to produce an instantaneous localized temperature increase: *(9)* estimate a localized temperature of 648°C when grinding olivine at ambient temperature in water with an atmosphere of CO_2, resulting in the production of light hydrocarbons (9-10).

Previous research has investigated mechanochemical CO_2 trapping through grinding of magnesium- and calcium-rich minerals (e.g., olivine, wollastonite and diopside) at ambient temperatures in dry, humid, or wet (H_2O) conditions within an atmosphere of pure CO_2 *(11-14)*. They achieve CO_2 trapping efficiencies between 5.4 and 123.0 $mgCO_2/g$ (*11-15*).

In this paper we investigate the mechanochemical CO_2 trapping capability of commonly available polymineralic rocks. We determine the concentrations of trapped CO_2, using rocks that are both high (basalt), and low (granite), in magnesium and calcium, and compare these results with experiments on the individual minerals from which these rocks are comprised. We also present data on the leachability of the mechanochemically trapped CO_2, for both the polymineralic rocks and the individual minerals.

Results

Our experiments investigated two rock types, basalt and granite, and the minerals orthoclase, oligoclase, olivine, biotite, clinopyroxene and quartz. Basalt and granite are common rock types that are very high and very low in carbonate-forming metals, respectively. We chose minerals that represent the most abundant rock-forming silicate minerals. To enable comparison of the results for polymineralic rock to those for individual minerals, aliquots of granite and basalt samples were analyzed for major oxides by X-ray Fluorescence (XRF) (Table S1) and for mineralogy by semi-quantitative X-ray diffraction (XRD) (Fig.1a, 1b, Table S2) analysis (ALSGlobal Ltd). As expected, XRF results (Table S1) for the major oxides show that CaO, MgO and Fe_2O_3 are high in the basalt (CaO = 9.75 wt%, MgO = 10.8 wt%, Fe_2O_3 = 12.27 wt%) and low in the granite (CaO = 0.83 wt%, MgO = 0.45 wt%, Fe_2O_3 = 2.08 wt%). XRD results show that the basalt is predominantly comprised of intermediate feldspar, clinopyroxene, olivine, with more minor micas, analcime and other clay minerals (Fig1a, Table S2). The granite was composed of over 50% intermediate feldspars, the rest being quartz and mica, with <1% of other minerals (Fig.1b, Table S2). Oligoclase has been selected to represent plagioclase for both basalt and granite since feldspars with varying compositions (oligoclase and labradorite) have previously been shown to capture similar amounts of CO_2 when milled (*13*).

To prepare samples for the mechanical activation experiments, mineral and rock samples were crushed using a hydraulic press, sieved to a grain size of <1mm, then dried at 105 °C for 12 hours. BET (Brunauer, Emmett and Teller) surface area analysis was carried out on all rock and mineral samples pre- and post-mechanical activation (Table S3). The mechanical activation experiments were conducted in two stages. First, to determine CO_2 trapping efficiency through mechanical activation, samples were milled in 99.995% CO_2 at 4 bar for 2.5 hours at 350 rpm using a planetary ball mill (see materials and methods for full details). No heating was applied during milling; however, frictional heating resulted in a final sample temperature of 52°C at the end of the 2.5 hours. Control samples for all rocks and minerals used the same methodologies for both stages of the process but were milled in air (which contains ~0.04% CO_2) instead of being milled in 99.995% CO_2. The average particle size for granite and basalt after milling were 15.9 µm and 14.8µm respectively (FigS3). Second, aqueous leaching experiments were carried out on the mechanochemically activated powders, to compare how much carbon remains trapped after being reacted with water in the rocks and the minerals over a 24-hour period. Rock and mineral powders were leached in air-equilibrated deionized water using a water-rock ratio of 10:1 in an end-over-end shaker for 24 hours. The resultant supernatant was tested for dissolved magnesium

and calcium by inductively coupled-optical emission spectroscopy (ICP-OES) (Table S7). The leachate was recovered, dried at 45°C, and tested for carbon concentration using a CHN (carbon, hydrogen, nitrogen) analyzer.

The mass of CO_2 captured during ex-situ mechanochemical activation of the rock and mineral samples milled in CO_2 is shown in Fig.1c (solid bars), compared to the CO_2 captured in the controls (milled in air, pale solid bars). Rock and mineral samples were analyzed post-milling for carbon content using a CHN analyzer (detection limit 0.1 $mgCO_2/g_{rock}$). Figure 1c shows that the basalt and the granite capture 15.5 and 13.9 $mgCO_2/g_{rock}$ of CO_2 respectively. Normalizing these findings to the BET-specific surface area created by the milling shows that 3.0 $mgCO_2/m^2$ has been captured in the basalt, as compared to 1.8 $mgCO_2/m^2$ in the granite (Table S3). Analysis of the CO_2-activated rock powders (and the controls) using both Fourier Transform Infra-red spectroscopy (FTIR) and XRD spectra, showed that no carbonate minerals had been created; there were no changes to the mineral types present in the samples (Fig.S1 and S2).

Figure 1d presents similar data for the individual minerals: Olivine and biotite trap the most CO_2, trapping 9.5 $mgCO_2/g$ and 9.2 $mgCO_2/g$, respectively, which is consistent with published trapping efficiencies of between 5.4 and 26.0 $mgCO_2/g$ *(12-18)* for magnesium- and calcium-rich minerals. Oligoclase and clinopyroxene capture a small mass of CO_2; 2.0 $mgCO_2/g$ and 1.8 $mgCO_2/g$, respectively and Quartz captures 1.1 $mgCO_2/m^2$ of CO_2. Orthoclase traps no CO_2.

From the FTIR data none of the mineral samples resulted in the formation of new carbonate minerals.

Aqueous leaching experiments were conducted on all samples after milling (Fig.1c, 1d, Table S4) to determine how vulnerable the mechanochemically trapped CO_2 is to dissolution; if the trapped CO_2 is insoluble then the crushed rock can be used, or stored, anywhere in the environment without releasing CO_2 when wet. The mass of carbon remaining in the powders after leaching was determined from carbon analysis. The residual carbon content of the rocks and minerals after leaching is shown in Fig. 1c; 98% of carbon is retained in the basalt and 96% in the granite. This is in stark contrast to the results for the individual minerals. Olivine and biotite, the minerals that trap the most CO_2, retain only 7.4% and 40.7% respectively after leaching. Clinopyroxene retains 61.1% of carbon and oligoclase and quartz have the same carbon content pre- and post-leaching. To check that CO_2 leaching had reached an equilibrium in the granite and basalt powders, a time series experiment was conducted with samples taken at 0, 1, 2, 4, 12 and 24 hours. No significant change in the carbon content of the powders was visible between samples after 1 hour of leaching and 24 hours (Table S5). Carbon content of the basalt and granite powders after 24 hours of leaching was also determined for experiments with an increased powder-to-water ratio of 1:100. Again, no change in the carbon content of the powders was observed (Table S6).

Leachates were monitored for the dissolution of the common carbonate-forming metals, calcium and magnesium. Analysis shows an increase in calcium (Fig.2a and 2c) and magnesium (Fig.2b and 2d) leaching for all rocks and minerals milled in CO_2, when compared with the control (Table S7). For the basalt and granite this increase is large. The CO_2-activated basalt samples leach ~6 times more calcium and ~14.9 times more magnesium than the control basalt samples. In the CO_2-activated granite samples, ~3 times more calcium is leached and ~9 times more magnesium (Fig. 2a and 2b). At first glance, results for the individual minerals (Fig.2c and 2d) look similar; there is an increase in the calcium and magnesium leached from the CO_2-activated samples in comparison to the controls (with the exception of calcium leaching from biotite). However, the mass of calcium leached from the minerals is an order of magnitude lower than that leached from the rocks. In contrast, for the minerals containing magnesium, the leached mass of magnesium is an order of magnitude higher than that leached from the rocks.

Cation leaching from the rocks could provide an additional store of CO_2 as the leached ions can combine with CO_2 to precipitate carbonate minerals. This leads to an increase in the total CO_2 trapping potential of the basalt and the granite, through application of a three-stage process (1) direct capture of CO_2 via mechanical activation (2) leaching of dissolvable metals into solution (3) aqueous carbonation via injection of CO_2 gas into the leachate. Based on the leachate data in Table S4 & S7, the three stage process results in a final total trapping potential of 19.6 mg/g CO_2 for the basalt and 14.5 mg/g CO_2 for the granite, assuming the final products are washed prior to use and all the calcium and magnesium in solution used for additional aqueous carbonate precipitation (Fig.2e).

To elucidate CO_2 trapping mechanisms within the rocks and minerals, thermal desorption experiments were carried out using coupled pyrolysis-gas chromatography-mass spectrometry (Py-GCMS). Thermal desorption is a process whereby samples are gradually heated (up to 1000°C) and CO_2 release is measured as a function of temperature. The resulting desorption profile reflects the kinetic energy required to break each type of bond. Carbon that is physically bound (as CO_2 molecules held by weak intermolecular forces) will be emitted at temperatures less than or equal to 115°C (*16*). An individual type of carbon bond, such as a calcium carbonate, produces a desorption profile that rises and falls around a single, known peak temperature. The temperature of the peak represents the average thermal energy required to break each bond, so is an indication of the chemical bond strength. If several types of carbon bond are present within a rock or mineral, then the resulting thermal desorption profile will be a linear superposition of the individual peak profiles for each type of carbon bond.

All rock and mineral samples were tested for thermal desorption prior to, and after, leaching (including the controls). Samples were heated from 40°C to 1000°C with a temperature ramp of 20°C per min. The evolved CO_2 gas given off was measured directly by the mass spectrometer. Between one and four peaks can be identified in each sample (Fig.3), with consistent values of 400°C, 625°C, 800°C and 875°C. The common carbonate minerals $MgCO_3$, $CaMg(CO_3)_2$, and $CaCO_3$ have known peak thermal decomposition equilibrium temperatures of 310°C, 538°C and 844°C, respectively where CO_2 is emitted as the carbonate minerals are broken down (*17*). Hence, the thermal desorption profiles in Fig.3 are not formed by superposition of carbonate peaks and are consistent with the XRD analysis, i.e., no carbonate minerals are present in the samples prior to or after mechanochemical CO_2 activation.

A comparison of the thermal desorption profiles of the CO_2-activated samples (Fig.3, blue and red lines) and the controls (Fig. 3, black lines) shows a difference in profile shape for all the rock and mineral samples that trap significant carbon; the CO_2-activated samples have a greater number of distinguishable peaks (carbon bond types) than the equivalent control. In the mineral samples, the desorption profiles appear to be largely a superposition of between one and four distinct peak profiles (i.e. carbon bonds), whereas the polymineralic rocks appear far more heterogeneous, with a greater volume of CO_2 being emitted over a wide

temperature range: in the basalt CO_2 is emitted from 300-850°C and there are no dominant peaks; in the granite CO_2 is emitted from 300-650°C with one peak at 400°C. Finally, in both rocks the shape of the desorption profiles before and after leaching (blue and red lines respectively) remains largely unchanged, whereas in the pure mineral systems, some peaks are entirely removed or very significantly reduced after leaching e.g., the peaks at 800°C and 875°C in the olivine. This implies that some carbon bonds within the individual mineral samples are highly soluble, but not in the polymineralic rocks (see 800°C in the basalt, Fig.3a). Also evident for the granite samples in Figure 3b, is an apparent reduction in the total carbon released after leaching; this is despite their similar measured carbon contents (Fig.1c). This occurs if the aliquot sampled from the 'after leaching' powder contained a higher proportion (by mass) of larger particles, and thus a smaller total surface area for CO_2 trapping.

Discussion

Previous studies of the potential for carbon capture through direct gas capture, via mechanochemical reactions in calcium- and magnesium-rich minerals, suggest that CO_2 is captured into the crushed rock by a carbonation process *(11-14)* and that this results in carbonate ion formation *(11,13)*. Our experiments show that carbonates are not produced. The XRD results and thermal desorption profiles both indicate that carbonate minerals are not detected. The high efficiency of granite (Fig.1c) as a carbon capture material, when it contains no significant quantities of calcium, magnesium or other key carbonate-forming metals also confirms that the mechanism of trapping does not involve metal carbonate formation. Since there is no evidence of new mineral formation, alternative trapping mechanisms must be responsible. Likely trapping mechanisms include mechanochemical-induced adsorption of CO_2 onto the rock/mineral surface or mechanochemically-induced diffusion of CO_2 into the near-surface of the deformed crystal lattice. During adsorption the CO_2 becomes attached chemically or physically bound to the rock/mineral. CO_2 molecules are physically attached to the mineral surfaces in multiple layers by weak intermolecular Van Der Waals forces (*18*). Physical sorption of CO_2 onto a mineral surface can occur at low temperatures (*18*) requiring little activation energy compared with chemical sorption. However, these weak forces are readily reversible and would result in a significant thermal desorption peak at temperatures less than or equal to115°C (*16*), which is not observed. Chemisorption (or chemical adsorption) requires activation energy and typically occurs at much higher temperatures (400-600°C, (1-4, 6)) than those measured after milling (~52°C). However, this thermal energy requirement could be replaced by work done during the mechanochemical activation process. During mechanochemical activation, bonds are broken within the rock, forming surface radicals and positive and negative surface charges on the crystal surface *(8-9, 19, 20)*. Instantaneous, highly localized temperature increases may also occur of >600ºC *(9)*. The presence of broken bonds also decreases the activation energy required for CO_2 to form chemical bonds with positively and negatively charged species within the lattice. Deformation of the mineral surface facilitates tribodiffusion and trapping of CO_2 molecules into the silicate mineral lattice (*21*). Once adsorbed, the chemically bonded CO_2 will require considerable energy input (heat or chemical) to desorb the bonded and tribodiffused gas molecules. Thus, a mechanochemical adsorption mechanism is consistent with the observed thermal desorption profiles, in which CO_2 is released at temperatures between 300°C and 900°C. The distinct peaks observed in the desorption profiles represent different locations for chemisorption of CO_2 in the crystal lattice; since different locations in the lattice will require different amounts of activation energy to break the bond and release the CO_2.

Results from the mechanochemical activation experiments, leaching experiments and thermal desorption experiments all indicate that polymineralic systems behave differently to monomineralic systems. The majority of CO_2 trapped in the granite and basalt is insoluble, whereas in the individual minerals the majority of CO_2 trapped is primarily soluble. From the mineral compositions of the basalt and the granite (Table S2, Fig.1a, 1b) it is possible to estimate the likely CO_2 trapped in each rock as a weighted sum of the CO_2 trapped in the individual minerals and then to compare it to the observations for each rock-type (Fig.1e). Figure 1e shows that the concentration of trapped CO_2 in the basalt is 4.2 times the predicted value based on mineral composition alone, and 5.9 times the predicted value for the granite. A similar estimate can be made by comparing estimated and observed values post-leaching (Fig.1f). Here, the difference between the CO_2 remaining in the granite and basalt after leaching, and a weighted sum of their mineral compositions, is even more pronounced: 10 times more CO_2 remains in the basalt after leaching than predicted from mineral composition alone and over 6 times more in the granite. The difference between observed and predicted concentrations of calcium and magnesium in the leachate are similarly stark (Fig.S3a and S3b): far more calcium than predicted, and less magnesium, is leached from both rocks based on their respective mineral compositions.

The observed differences between the polymineralic and monomineralic systems suggest that in polymineralic rocks, chemical adsorption preferentially occurs at grain boundaries between mineral types i.e., at the interfaces between different types of crystal. Since many possible combinations of crystals could interface in a polymineralic rock, many different carbon bonds and therefore bond strengths are possible, each of which will require a different energy to break the bond. This explains the paucity of clear peaks in the thermal desorption data for rocks. It is known that secondary minerals in polymineralic rocks significantly affect the bulk ductile deformation behavior of rocks, and consequently their microstructure (*22*). At a larger scale, deformation has been shown to be localized at interfaces between materials with different mechanical properties where the stress concentrations develop (c.f. (*23*)). We speculate that at the micron-scale grain boundaries between different minerals which have different mechanical properties, also act to concentrate stress. Therefore, polymineralic rocks undergo more lattice deformation along grain boundaries than monomineralic rocks, for the same amount of mechanical energy input during milling, and hence trap more CO_2.

We propose the following mechanism for mechanochemical trapping of CO_2. Mechanical activation deforms the crystal lattice, preferentially at the boundaries between different minerals. When a mineral is deformed, dislocations in the crystal lattice migrate to the mineral surface, generating charged species. If bonds break during fracturing, a localized instantaneous temperature rise occurs, surface radicals form, and charged silica and oxygen become available (*24*). We propose that both surface radicals and charged species lower the activation energy required for CO_2 chemical adsorption to the surface and promote diffusion of CO_2 into crystal lattice interstitials (*24*). The resulting bonds between the CO_2 and the charged mineral surfaces are extremely strong, meaning that the adsorbed CO_2 is relatively insoluble. Our results indicate that

the presence of CO_2 in the lattice weakens the bonds holding some ions in the lattice thereby releasing more calcium and magnesium into solution during leaching. When reacted with water, the weakened bonds are easily broken; thus, in the polymineralic rocks, more calcium and magnesium ions are dissolved into solution. Serendipitously, this increase in the leaching of calcium and magnesium provides additional CO_2 trapping potential (Fig.2e) in the form of aqueous carbonate precipitation.

The potential impact of mechanochemical carbon trapping on global CO_2 emissions could be approximated, theoretically, based on plausible assumptions. If existing polymineralic rock milling processes, such as the production of powders for the chemical and cosmetic industries, and the production of aggregates for construction, were to incorporate mechanochemical trapping of CO_2 this would not incur significant additional energy expenditure. Estimating the amount of CO_2 trapped if these milling processes were conducted within a CO_2 atmosphere, instead of air, requires data on the annual production of aggregates and powders from polymineralic metamorphic and igneous rocks. We have not found a reliable source of these data globally, instead we use published data from Norway, which produces 52Mt/y of hard rock (metamorphic and igneous rocks) aggregate (25). Research shows that for every 100Mt of saleable igneous and metamorphic aggregate, approximately 25Mt of fines are produced (26). Based on our research, a change in surface area of 5.4-7.8 m^2/g results in a CO_2 capture potential of 14.5 - 19.6 $kgCO_2$/tonne (Figure 2e including aqueous trapping), so 25 Mt of rock fines would trap 0.4-0.5Mt of CO_2. Hence, if hard rock crushing facilities for construction aggregate in Norway could be adapted for mechanochemical CO_2 capture, this would equate to 0.19-0.26Mt of CO_2, or approximately ~0.4%-0.5% of Norway's 2021 annual CO_2 emissions (48.9Mt) (27). The amount of CO_2 trapped by mechanochemical reactions depends directly on the additional surface area created during milling. Based on an assumption of spherical particles, for every order of magnitude reduction in particle size, there is an order of magnitude increase in surface area. In our experiments, the median particle size was reduced by one order of magnitude (Fig. S4) which resulted in a measured change in surface area of 5.4-7.8 m^2/g. Optimizing milling processes to produce finer rock powders (e.g. for the chemical industry or as a cement replacement material (28)) would result in significantly higher CO_2 capture potential per unit mass of fines. To optimize CO_2 capture potential in industrial aggregate and powder production, further research should focus on an assessment of the energy required for additional milling, against the time-varying rate of CO_2 trapping.

Our research shows that during mechanochemical CO_2 trapping experiments, polymineralic rocks outperform individual minerals in terms of both the amount of CO_2 captured and the subsequent leachability, making them viable substrates for carbon capture and future study. Experiments conducted in ambient temperature conditions show that basalt and granite can trap 15.4 $mgCO_2/g$ and 13.9 $mgCO_2/g$, respectively when dry milled in gaseous CO_2. We demonstrate through XRD analysis and thermal desorption, that the mechanism for mechanochemical trapping of CO_2 in rocks and minerals is not, as previously thought, in the form of carbonate mineral production. Rather, our experiments suggest that mechanochemical trapping occurs via chemical adsorption of carbon within the mineral lattice, which preferentially occurs on grain boundaries. A comparison of the carbon trapped in polymineralic systems (basalt and granite) with that trapped in pure mineral systems, shows that polymineralic rocks trap significantly more CO_2 than would be expected from their mineral composition. We show that mafic minerals, previously proposed as mechanochemical substrates, leach 60%-93% of their trapped carbon when mixed with water. By contrast, the CO_2 trapped in polymineralic rocks is poorly soluble, 2% is leached from the basalt and 4% from the granite, and hence the resulting materials form a usable and resilient product. Based on our findings, for every 100 Mt of saleable hard rock aggregate 0.4-0.5 $MtCO_2$ could be trapped into quarry fines, as a byproduct of existing global aggregate production.

Methods

Materials and Preparation

Two silicate rock types were chosen for the experiments (Basalt and Granite) and minerals quartz, oligoclase, orthoclase, olivine (fosterite), biotite, and clinopyroxene (aegirine). Certified mineral samples were used (UKGE Ltd.) except for quartz, which was derived from a quartz sandstone (Table S2). Each rock and mineral type was processed in a hydraulic press and the fragments sieved to a particle size 212μm-1000μm, the particle size distribution of the granite and basalt are given in Figure S3. The sieved fraction was rinsed in deionized water and dried at 105°C for 24h. Following crushing, a portion of each rock was analyzed by ALS Environmental Ltd. for mineralogy via semi-quantitative XRD and rock analysis using XRF to characterize the starting rock material used in rock comminution experiments. Sandstone (quartz) samples are comprised of 99% quartz and less <1% other impurities (Table S2) and is referred to as quartz. Experiments are carried out under two different gases carbon dioxide (CO_2, 99.995%) and air (at room temperature, humidity, and pressure), to determine the carbon capture potential of silicate rocks during mechanical grinding.

Rock/Mineral Comminution Experiments

Mechanical activation of each rock type (Basalt, Granite, and individual minerals) under different atmospheres Carbon Dioxide (CO_2) and atmospheric air control were carried out in a PM100 planetary ball mill (Retsch). Milling in air is used as a control since current industrial rock milling processes mill in air. Hence, any additional CO_2 trapped, above the control values, represents additional CO_2 that could be trapped, as a by-product, in existing aggregate and powder production processes. Milling experiments used a 250ml stainless steel grinding jar with aeration cover to allow for milling under different gas atmospheres and variable gas pressures. The ball mill and grinding balls were cleaned for rock/mineral comminution experiments by washing with 5 % decon solution, rinsing with deionized water and drying, milling 10 g of rock for 10 minutes and discarding the crushed material. To ensure a consistent moisture content between experiments, following cleaning, the grinding jar was loaded with 60g of the same rock type, heated to 105 °C for 2h, sealed with the aeration cover and allowed to cool prior to milling. Control samples were sealed in air under atmospheric pressure, while experiments under different 100% atmospheres (either CO_2 or air) were prepared by removing any air from the grinding jar, flushing the reactant gas through the grinding jar, pressurizing the outlet to the jar to 4 bars with the reactant gas and sealing. This process of atmospheric 'pre-flushing' ensured consistent atmospheric conditions between experiments. Milling was carried out with a ball to rock ratio of 10:1 (w:w) at 350 rpm for 2.5 hours with direction reversal every 10 minutes. These parameters were selected as they are similar to the conditions used in past mechanochemical CO_2 capture experiments (*11*). A grinding time of 2.5 hours was chosen both to be comparable to

previous mechanochemical investigations (13, *19, 20*) and because past research (*4-6*) has shown that further milling, under the same mill conditions, does not produce increased surface area. After milling for 2.5 hours the ball mill was left for a further two hours for the samples to reach room temperature. Milling experiments were carried out in duplicate under each atmospheric condition.

Characterization Methods

Post-grinding analysis of the crushed samples is used to characterize the concentration of carbon trapped in the samples under different atmospheres and determine any mineralogical changes to the rocks and minerals. Elemental analysis for carbon was carried out on all powdered rocks and minerals by Edinburgh University using Thermo Fischer Scientific Flash SMART elemental analyzer fitted with a 2m CN/CHN stainless steel separation column and CN/CHN prepacked quartz reaction tube. Four-point calibration was performed using different masses of Atropine. Where samples were lower than or close to the level of detection (1.0 $mgCO_2/g$) additional analysis was performed at the university of Strathclyde using Exeter Analytical CE440 Elemental Analyzer with a lower detection limit (0.1$mgCO_2/g$) to confirm the results. Both elemental analyzers ensure all elemental carbon within a sample is converted to CO_2 and measured using a series of thermal conductivity detectors to determine the concentration of elemental carbon within a sample. Analysis of the air milled control samples (where CO_2 is at ambient concentration ~400 ppmV) gives a control carbon measurement for each sample, which the CO_2 milled samples can be compared against. XRD analysis of the rocks shows no carbonate minerals are present within the samples, hence, we assume that all elemental carbon within the rock is taken from the CO_2 atmosphere.

Powdered minerals and rocks are analyzed spectroscopically by Attenuated Total Reflection Fourier Transform Infer Red (ATR-FTIR) spectroscopy using a Thermofischer Nicolet i5 with a range of 100-4000 cm^{-1}. X-ray Diffraction (XRD) was performed on the basalt and granite using BRUKER D8 ADVANCE with DAVINCI X-Ray Diffractometer. XRD parameters were as follows; scan range of 5-60 2θ, a step-size of 0.01 and a dwell time of 1 second. Physical changes, surface area and particle size distribution were measured by BET analysis (Micrometrics ASAP2020) and Mastersizer 2000 (Malvern) respectively. Surface area (Table S3) and particle size distribution (Fig. S3) were measured in granite and basalt before milling and after milling and change in surface area calculated.

Stability of Captured Gases

Reacted rock samples were tested by thermal desorption and leaching to determine the longevity of GHG captured into both monomineralic and polymineralic systems.

Thermal desorption experiments carried out using Pyrolysis Gas Chromatography Time of flight mass spectrometry (Py-GC-ToFms). The CDS 6000 pyrolysers is connected to an Agilent 9800-A gas chromatograph via a transfer line heated to 310 °C connected to a split inlet at the same temperature. A 1m 0.18 µm fused silica capillary connected the pyrolyser directly via a heated transfer line to a Pegasus 4D time of flight mass spectrometer (LECO St. Josephs Michigan). The GC oven temperature was set to 310 °C and the helium flow rate set to 1ml/min with a split ratio of 75. The spectra acquisition range was set 30-550 at a sample rate of 10 spectra per second. Rock and mineral samples were weighed (5mg +-0.2mg) using a microbalance into Quartz tubes and packed with quartz wool to keep the samples in the tubes. Each Quartz tube was heated in the pyrolyser from 40 to 1000 °C at a heating rate of 20 °C/min and the evolved gas measured by the mass spectrometer, thermal desorption experiments were continued to the upper limit of the instrument (1000 °C). Samples were run in duplicate as well as blanks consisting of empty quartz tubed packed with quartz wool. All samples were run as a single batch, without adjustment to the analytical equipment. Samples are therefore comparable in terms of the relative mass emitted at a given temperature (i.e., the shape of the thermal desorption profile). The total mass of CO_2 emitted from each sample cannot be accurately determined (this is determined using the CHN analysis). The thermal desorption data was processed in R, the baseline for m/z 44 (CO_2) was corrected based on analytical blanks and the signal smoothed using a moving average.

Leaching experiments were carried out by placing 4.5g of rock and mineral samples into 50ml HDPE centrifuge tubes with 45ml of ultra-pure water equilibrated with atmosphere for 24h. The centrifuge tubes were agitated in an end over end shaker for 24h at a rate of 10rpm. Following agitation, the centrifuge tubes were centrifuged at 4629 g for 10 minuets, the supernatant was syringe filtered through 0.45um cellulose acetate filters, then measured for cations Ca^{2+} and Mg^{2+} using ICP-OES. Method blank samples containing 50ml of water were also analyzed. Each experiment was carried out in duplicate, and each sample tested by ICP was tested in triplicate. Results in Table S5 are the mean concentration alongside the standard deviation. Cation analysis was carried out using ICP-OES (ThermoFisher). The substrate was dried at 45°C for 24 hours and analyzed using a CHN analyzer and Py-GC-ToF to determine the carbon content and thermal stability of trapped carbon remaining in the rock after leaching. Additional time series leaching experiments were performed on the Granite and Basalt. Time series experiments were prepared as above with two samples of granite and basalt prepared for each time point (0, 1, 2, 4,12 and 24hours). Each time point sample was then analysed in duplicate by elemental analyzer (i.e. by collecting two separate sub-samples of the powdered rock from each centrifuge tube) resulting in four carbon measurements for each time point, two from sample 1 and two from sample 2. Results for the 24-hour time series leaching experiment are presented in table S6. A final leaching experiment was carried out on the basalt and granite powders using a rock to water ratio of 1:100 following the same method as above but placing 0.45g of powder into the centrifuge tube with the same volume of water. Results for the rock to water ratio 1:100 are presented in table S6.

Calculation of aqueous carbonation potential

Aqueous carbonation potential was calculated by assuming that all the dissolved calcium and magnesium leached from the rock is combined with CO_2 to produce magnesium carbonate and calcium carbonate (i.e., if one mole of calcium and one mole of magnesium was leached two moles of CO_2 could be trapped as a metal carbonate). Calculation of the maximum mass of CO_2 which could be trapped as calcium and magnesium carbonate are displayed in equation 1.

$$Mass\ CO_{2\ (mg/g)} = \left(\frac{Ca\ concentation\ (mg/g)}{40\ (g/mol)} + \frac{Mg\ concentration\ (mg/g)}{24.3\ (g/mol)}\right) \times 44.1\ (g/mol) \quad (1)$$

Equation 1 calculates the total maximum mass of CO_2 which could be captured as magnesium and calcium carbonates. The total amount which can be captured in practice will depend on the partial pressure of CO_2 in the solution and the solution pH; aqueous carbonation reactions

are favored in high pH solutions, so to achieve this maximum value may require pH adjustment.

Data Availability Statement

All data that support the findings in this paper are available within the article and its Supplementary Information.

Acknowledgements

This version of the article has been accepted for publication, after peer review but is not the Version of Record and does not reflect post-acceptance improvements, or any corrections. The Version of Record is available online at:http://dx.doi.org/10.1038/s41893-023-01083-y. Use of this Accepted Version is subject to the publisher's Accepted Manuscript terms of use https://www.springernature.com/gp/open-research/policies/acceptedmanuscript-terms

This work was part-funded by the Engineering and Physical Sciences Research Council's Doctoral Training Awards Grant EP/M506643/1. Professor Lunn is funded by a Royal Academy of Engineering Research Chair. We would like to thank Prof William Sloan for his helpful input on the manuscript.

Author Contribution Statement

MS and RJL conceived the concept for the article and designed the experiments. MS performed the experiments. Results were analyzed and interpreted by MS, RJL and ZKS. RJL supervised the research. MS and RJL co-wrote the manuscript with significant contributions from ZKS. All authors discussed the results, commented on, and reviewed the manuscript.

Competing interest statement

The authors declare no competing interests.

Figure Legends/Captions

Figure 1. XRD mineral composition of (a) basalt and (b) granite. (c) The mean carbon concentration (crosses are the two experimental replicates) in basalt (green) and granite (purple) crushed in 99.9995% CO_2 before leaching (solid colors) after leaching for 24hours (horizontal lines) and crushed in (~400 ppmV CO_2) air before leaching (control, pale colors) and after leaching (vertical lines). (d) The carbon concentration of mechanochemically reacted minerals in CO_2 before and after leaching and in air. The measured vs predicted mechanochemically-trapped carbon concentration in rock, based on the weighted volume of minerals, before (e) and after (f) leaching.

Figure 2. Calcium (a) and magnesium (b) leached from basalt (green) and granite (purple) milled in CO_2 (horizontal lined) and air (vertical lines) after 24-hours. Calcium (c) and magnesium (d) leached from minerals, milled in air and CO_2 after 24hours (note the different y-axis scales parts c & d). (e) Measured CO_2 concentration in rock samples before leaching (solid colors), and the CO_2 concentration in rocks after leaching (black-lined) plus the potential CO_2 captured by aqueous carbonation (grey).

Figure 3. Thermal desorption profiles of rock samples Basalt (a) and Granite (b) and mineral samples Biotite (c), Clinopyroxene (d), Olivine (e), Quartz (f), Orthoclase (g) and Oligoclase (h). Blue lines are thermal desorption profiles of rocks and minerals mechanically activated with CO_2 before leaching and red lines are after leaching. Black lines are the air-milled control samples of rocks and minerals before leaching. Arrows indicate the position of reference common carbonate minerals $MgCO_3$, $CaMg(CO_3)_2$, and $CaCO_3$ which have known peak thermal decomposition equilibrium temperatures of 310°C, 538°C and 844°C, respectively (*17*).

References

1. K. S. Lackner, C. H. Wendt, D. P. Butt, E. L. Joyce, D. H. Sharp, Carbon dioxide disposal in carbonate minerals, *Energy* ***20***, 1153-1170 (1995). doi.org/10.1016/0360-5442(95)00071.
2. K. S. Lackner, D. P. Butt, C. H. Wendt, Progress on binding CO_2 in mineral substrates, *Energy Conversion and Management*, ***38***, S259-S264 (1997). https://doi.org/10.1016/S0196-8904(96)00279-8.
3. I. Rigopoulos, K. C. Petallidou, M. A. Vasiliades, A. Delimitis, I. Ioannou, A. M. Efstathiou, T. Kyratsi, Carbon dioxide storage in olivine basalts: Effect of ball milling process, *Powder Technology*, ***273***, 220-229 (2015). https://doi.org/10.1016/j.powtec.2014.12.046.
4. I. Rigopoulos, M. A. Vasiliades, I. Ioannou, A. M. Efstathiou, A. Godelitsas, T. Kyratsi, Enhancing the rate of ex situ mineral carbonation in dunites via ball milling, *Advanced Powder Technology*, ***27***, 360-371 (2016). https://doi.org/10.1016/j.apt.2016.01.007.
5. I. Rigopoulos, A. Delimitis, I. Ioannou, A. M. Efstathiou, T. Kyratsi, E., Effects of ball milling on the carbon sequestration efficiency of serpentinized peridotites, *Minerals Engineering*, ***120***, 66-74 (2018). https://doi.org/10.1016/j.mineng.2018.02.011
6. I. Rigopoulos, K. C. Petallidou, M. A. Vasiliades, A. Delimitis, I. Ioannou, A. M. Efstathiou, T. Kyratsi, On the potential use of quarry waste material for CO_2 sequestration, *Journal of CO_2 Utilization*, ***16***, 361-370 (2016). https://doi.org/10.1016/j.jcou.2016.09.005.
7. Liu, X., Li, Y., Zeng, L., Li, X., Chen, N., Bai, S., He, H., Wang, Q., Zhang, C., A Review on Mechanochemistry: Approaching Advanced Energy Materials with Greener Force. Adv. Mater. **34**, 2022, 2108327. https://doi.org/10.1002/adma.202108327
8. Sanna, A.L., Carta, M., Pia, G. et al. Chemical effects induced by the mechanical processing of granite powder. Sci Rep **12**, 9445 (2022). https://doi.org/10.1038/s41598-022-12962-3
9. F. Torre, V. Farina, A. Taras, et al., Room temperature hydrocarbon generation in olivine powders: Effect of mechanical processing under CO_2 atmosphere. Powder Technology, **364**, 915-923 (2020). https://doi.org/10.1016/j.powtec.2019.10.080.
10. N. Gamba, V. Farina, S. Garroni, G. Mulas, F. Gennari, CO_2 storage and conversion to CH_4 by wet mechanochemical activation of olivine at room temperature, Powder Technology, **377**, 857-867 (2021). https://doi.org/10.1016/j.powtec.2020.09.039.
11. A. Kalinkin, Kinetics of carbon dioxide mechanosorption by Ca-containing silicates CO_2 released on heating of mechanochemically activated samples, *Journal of Thermal Analysis and Calorimetry*, ***95***, 105-110 (2009). https://doi.org/10.1007/s10973-007-8913-y
12. M.G. Nelson, Carbon dioxide sequestration by mechanochemical carbonation of mineral silicates, report, April 1, 2004, (https://digital.library.unt.edu/ark:/67531/metadc779600/: accessed February 1, 2023), University of North Texas Libraries, UNT Digital Library, https://digital.library.unt.edu; crediting UNT Libraries Government Documents Department.

13. A. M. Kalinkin, E. V. Kalinkina, O. A. Zalkind, Mechanosorption of carbon dioxide by Ca- and Mg-containing silicates and alumosilicates. Sorption of CO_2 and structure-related chemical changes, *Colloid J.* ***71***, 185–192 (2009). https://doi.org/10.1134/S1061933X09020069
14. K. L. Sandvik, R. A. Kleiv, T. A. Haug, Mechanically activated minerals as a sink for CO_2, *Advanced Powder Technology*, ***22*** 416-421 (2011). https://doi.org/10.1016/j.apt.2010.06.004
15. J. Li, M. Hitch, Mechanical activation of magnesium silicates for mineral carbonation, a review, *Minerals Engineering*, ***128***, 69-83 (2018). https://doi.org/10.1016/j.mineng.2018.08.034.
16. R. V. Siriwardane, M-S. Shen, E. P. Fisher, Adsorption of CO_2, N_2 and O_2 on natural zeolites, *energy and fuels*, ***17***, 571-576 (2003). https://doi.org/10.1021/ef020135l
17. M. Olszak-Humienik, M. Jablonski, Thermal behavior of natural dolomite. *J Therm Anal Calorim,* ***119***, 2239–2248 (2015). https://doi.org/10.1007/s10973-014-4301-6
18. C. Erkey, M. Türk, "Chapter 6 - Thermodynamics and kinetics of adsorption of metal complexes on surfaces from supercritical solutions", in *Supercritical Fluid Science and Technology*, (Elsevier, ***8***, 2021) pp. 73-127. https://doi.org/10.1016/B978-0-444-64089-5.00047-0.
19. M. Stillings, R. J. Lunn, S. Pytharouli, Z. K. Shipton, M. Kinali. R. A. Lord, S. Thompson, Microseismic events cause significant pH drops in groundwater, *Geophysical Research Letters,* ***48***, (2021). e2020GL089885, https://doi.org/10.1029/2020GL089885
20. J. Telling, E. S. Boyd, N. Bone, E. L. Jones, M. Tranter, J. W. MacFarlane, P. G. Martin, J. L. Wadham, G. Lamarche-Gagnon, M. L. Skidmore, T. L. Hamilton, Rock comminution as a source of hydrogen for subglacial ecosystems, *Nature Geoscience*, ***8***, 851-855 (2015). https://doi.org/10.1038/ngeo2533
21. A. M. Kalinkin, E. V. Kalinkina, O. A. Zalkind, T. I. Makarova, Mechanochemical interaction of alkali metal metasilicates with carbon dioxide: 1. Absorption of CO_2 and phase formation, *Colloid J*, ***70***, 33–41 (2008). https://doi.org/10.1134/S1061933X08010067
22. M. Herwegh, J. Linckens, A. Ebert, A. Berger, S.H. Brodhag, The role of second phases for controlling microstructural evolution in polymineralic rocks: A review, *Journal of Structural Geology*, ***33***, 1728-1750 (2011). https://doi.org/10.1016/j.jsg.2011.08.011.
23. H. Moir, R. J. Lunn, S. Micklethwaite, Z. K. Shipton, Distant off-fault damage and gold mineralization: The impact of rock heterogeneity, *Tectonophysics*, ***608***, 461-467 (2013). https://doi.org/10.1016/j.tecto.2013.08.043
24. P. Yu. Butyagin, Mechanochemical reactions of solids with gases, *Reactivity of Solids*, ***1***, 345-359 (1986). https://doi.org/10.1016/0168-7336(86)80026-2.
25. Directorate of mining with commissioner of mines at Svalbard, Geological survey of Norway. Mineral resources in Norway, Production data and annual report 2007. https://www.ngu.no/upload/publikasjoner/rapporter/2008/mineralresources_eng_2007.pdf
26. C. J. Mitchell, P. Mitchell, and R.D. Pascoe, 2008. Quarry fines minimisation: can we really have 10mm aggregate with no fines? In: Walton, Geoffrey, (ed.) Proceedings of the 14th Extractive industry geology conference. EIG Conferences, 37-44, 109pp. https://nora.nerc.ac.uk/id/eprint/4932
27. Statistisk sentralbyrå (Statistics Norway), Emissions to air. https://www.ssb.no/en/natur-og-miljo/forurensning-og-klima/statistikk/utslipp-til-luft (2022).
28. K. Kartini, M.S. Hamidah, A.R. Norhana, and A.R Nur Hanani, (2014). Quarry dust fine powder as substitute for ordinary Portland cement in concrete mix. *J. Eng. Sci. Technol*, *9*(2), pp.191-205.

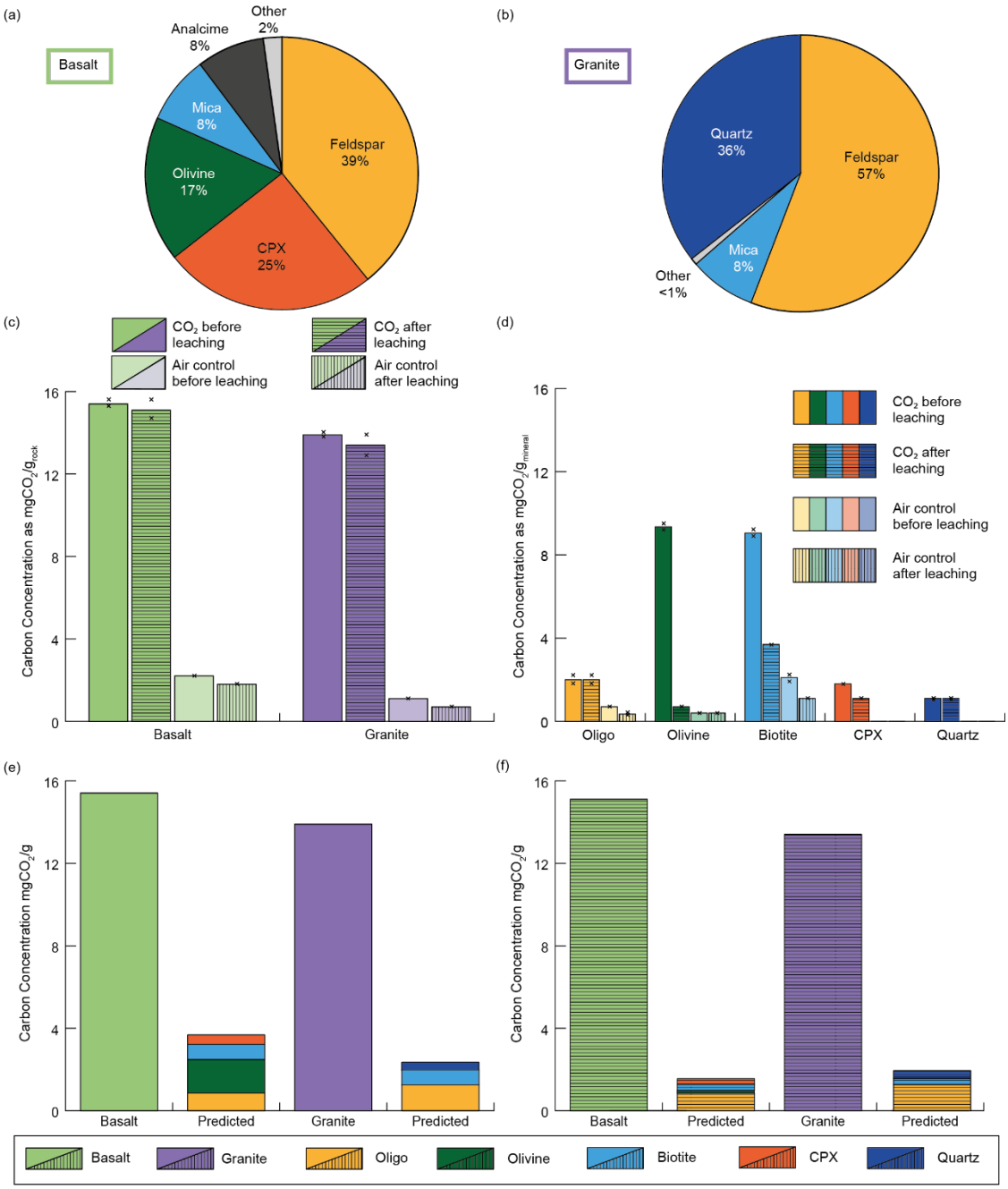
(a)
Basalt
Analcime 8%
Other 2%
Mica 8%
Feldspar 39%
Olivine 17%
CPX 25%
(b)
Granite
Quartz 36%
Feldspar 57%
Mica 8%
Other <1%
(c)
CO2 before leaching
CO2 after leaching
Air control before leaching
Air control after leaching
Carbon Concentration as mgCO2/grock
Basalt
Granite
(d)
CO2 before leaching
CO2 after leaching
Air control before leaching
Air control after leaching
Carbon Concentration as mgCO2/gmineral
Oligo
Olivine
Biotite
CPX
Quartz
(e)
Carbon Concentration mgCO2/g
Basalt
Predicted
Granite
Predicted
(f)
Carbon Concentration mgCO2/g
Basalt
Predicted
Granite
Predicted
Basalt
Granite
Oligo
Olivine
Biotite
CPX
Quartz

Figure 1

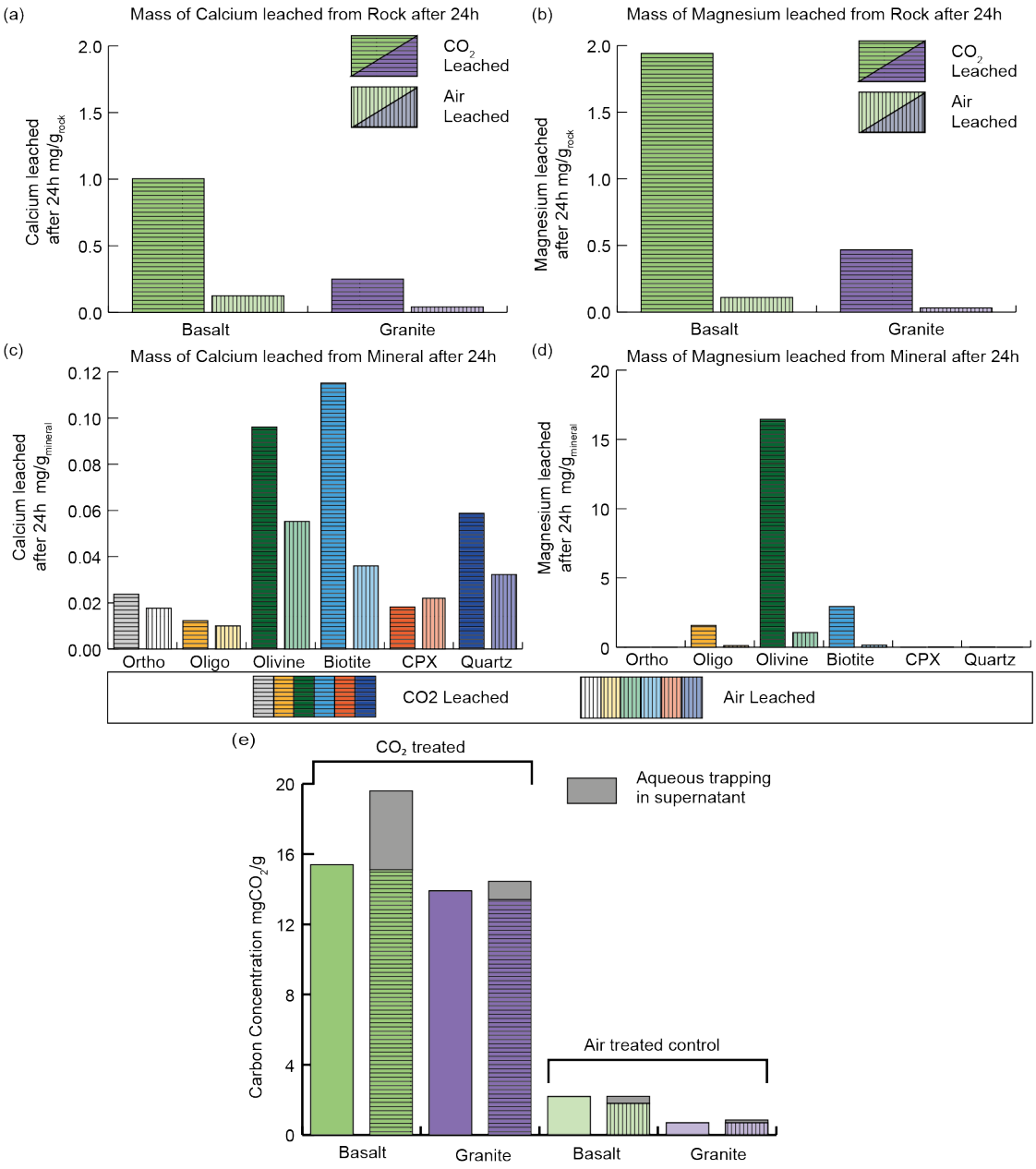
(a)
Mass of Calcium leached from Rock after 24h
Calcium leached after 24h mg/g rock
2.0
1.5
1.0
0.5
0.0
CO2 Leached
Air Leached
Basalt
Granite
(b)
Mass of Magnesium leached from Rock after 24h
Magnesium leached after 24h mg/g rock
2.0
1.5
1.0
0.5
0.0
CO2 Leached
Air Leached
Basalt
Granite
(c)
Mass of Calcium leached from Mineral after 24h
Calcium leached after 24h mg/g mineral
0.12
0.10
0.08
0.06
0.04
0.02
0.00
Ortho
Oligo
Olivine
Biotite
CPX
Quartz
(d)
Mass of Magnesium leached from Mineral after 24h
Magnesium leached after 24h mg/g mineral
20
15
10
5
0
Ortho
Oligo
Olivine
Biotite
CPX
Quartz
CO2 Leached
Air Leached
(e)
CO2 treated
Aqueous trapping in supernatant
Carbon Concentration mgCO2/g
20
16
12
8
4
0
Air treated control
Basalt
Granite
Basalt
Granite

Figure 2

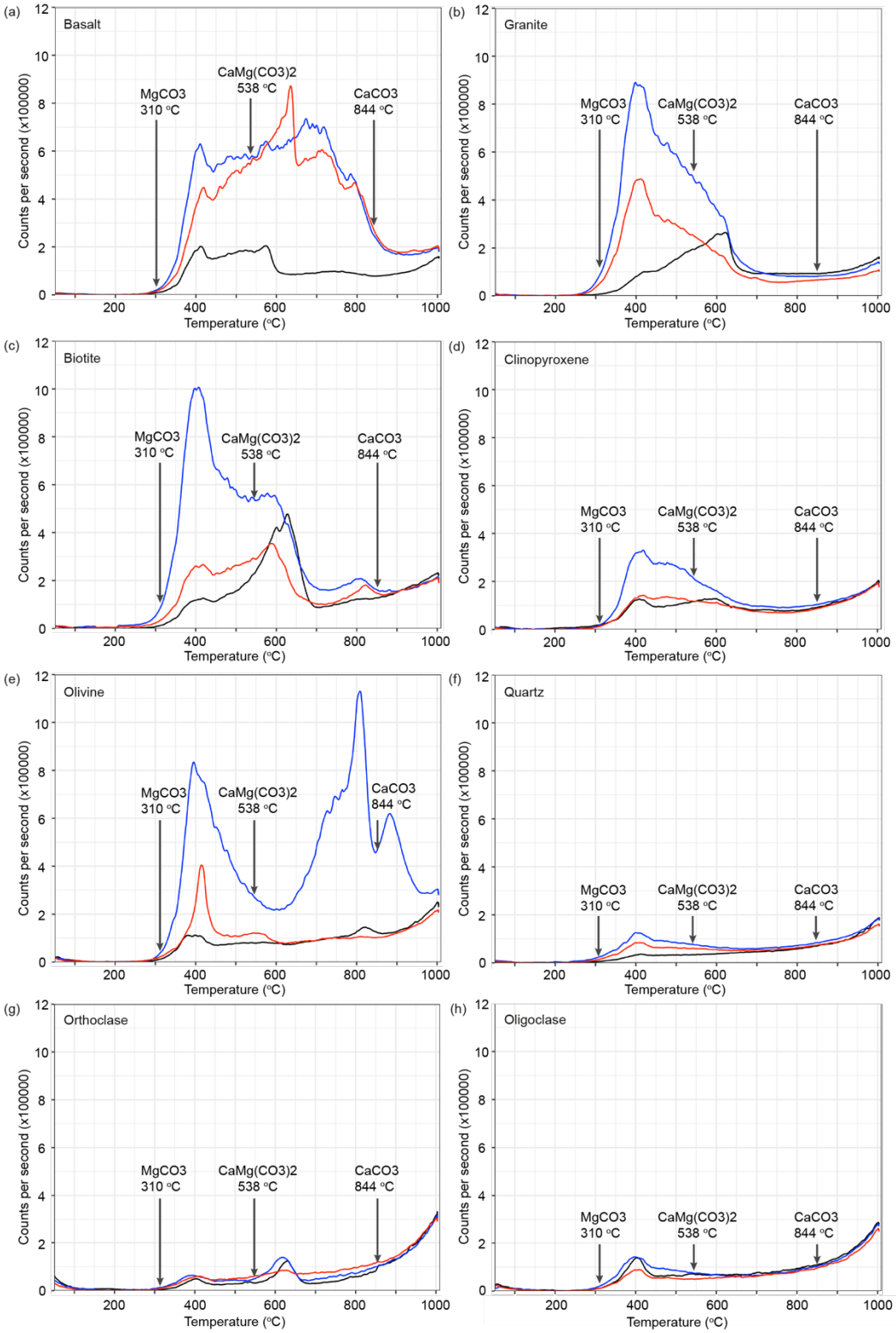
(a)
Basalt
(b)
Granite
(c)
Biotite
(d)
Clinopyroxene
(e)
Olivine
(f)
Quartz
(g)
Orthoclase
(h)
Oligoclase
MgCO3
310 °C
CaMg(CO3)2
538 °C
CaCO3
844 °C
Counts per second (x100000)
Temperature (°C)

Figure 3

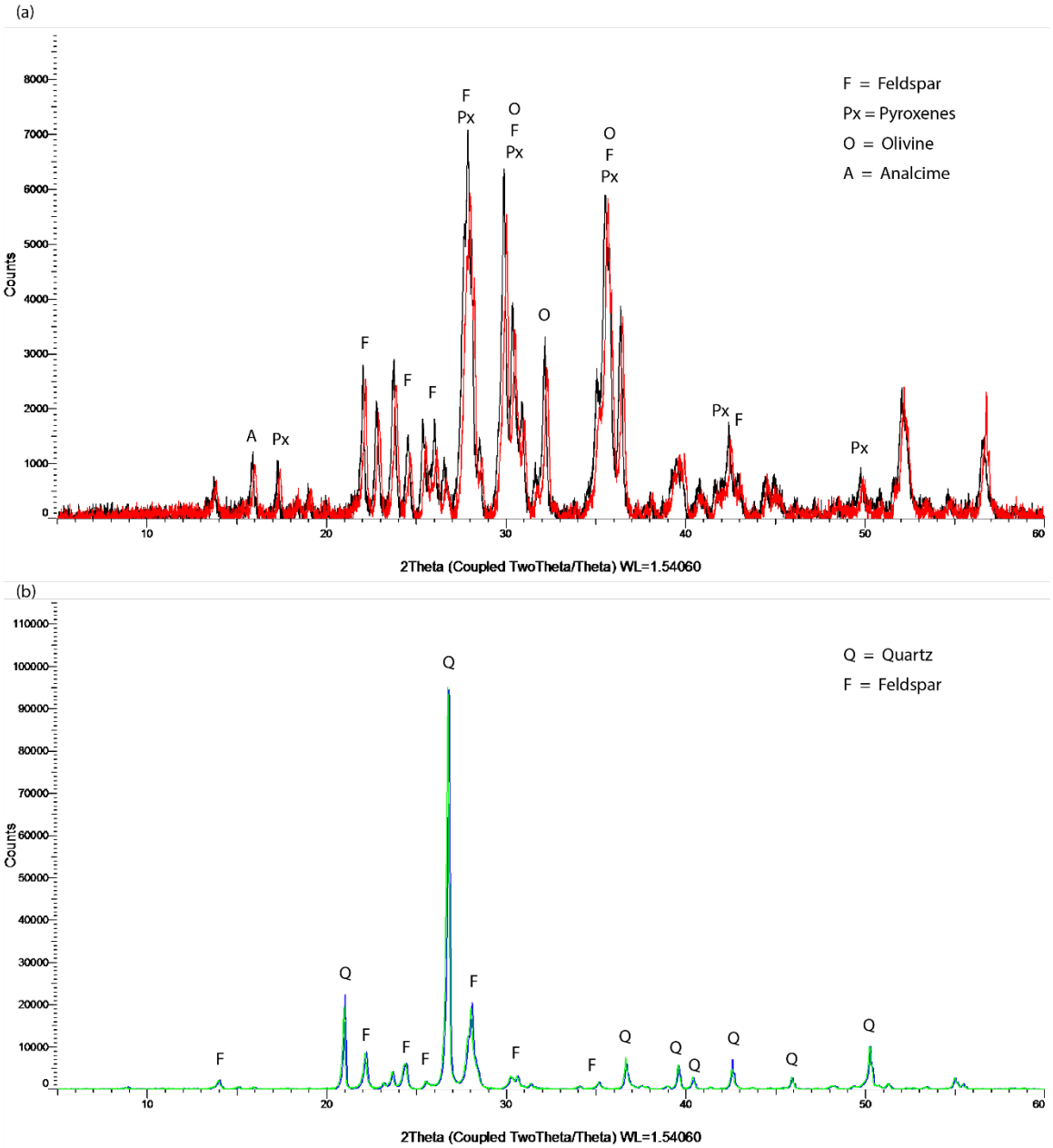

Fig. S1. XRD plots of rock after grinding in air (control) and CO_2, (a) Basalt (red) Air and (black) CO_2, (b) Granite (Blue) Air, and (Green) CO_2.

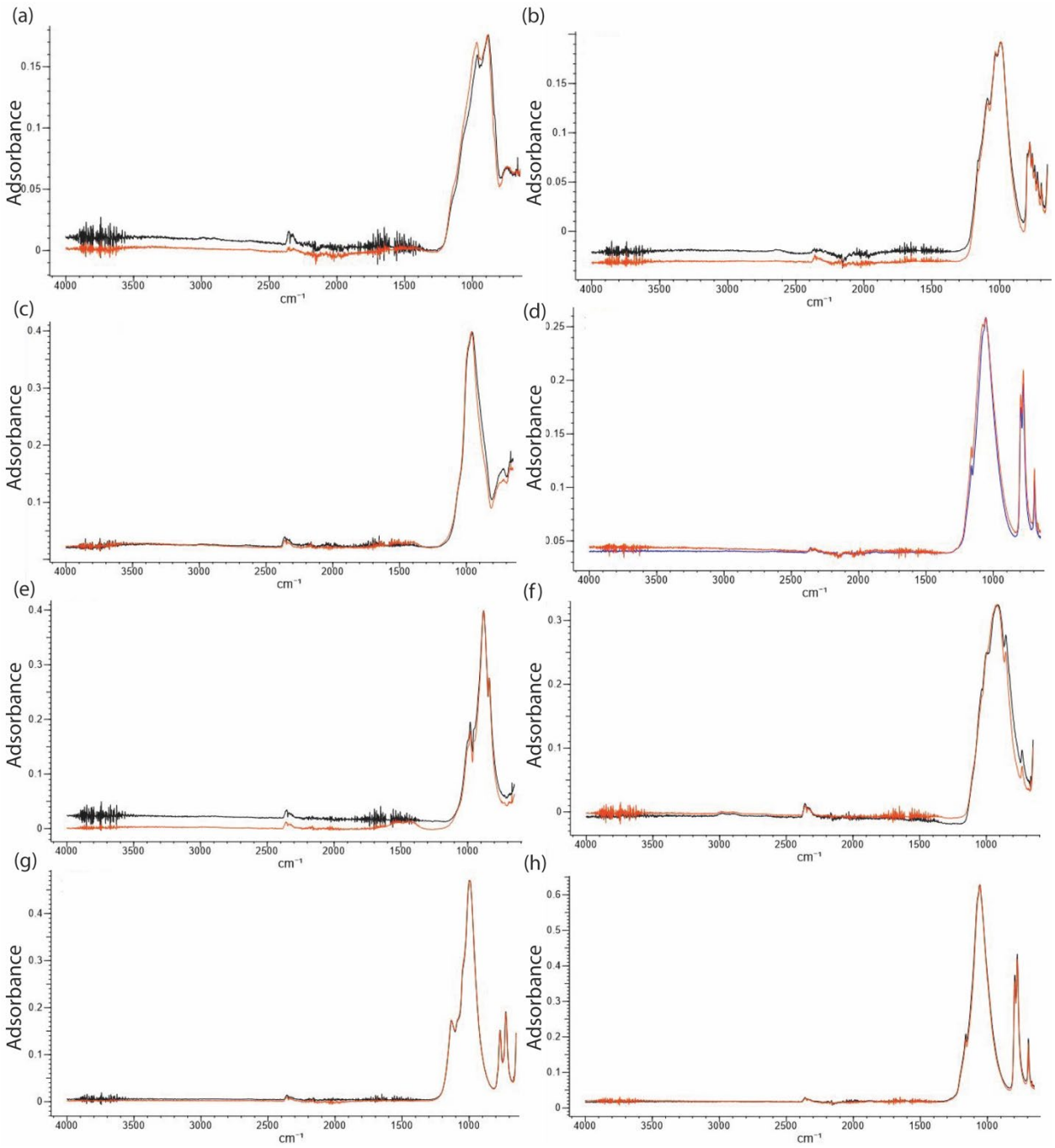

Fig. S2. FTIR spectra of rocks (a) Basalt, (b) Granite and minerals (c) Biotite, (d) Quartz, (e) Olivine, (f) Clinopyroxene, (g) Orthoclase and (h) Oligoclase, after mechanochemical activation in (red) CO_2, and (black) Air.

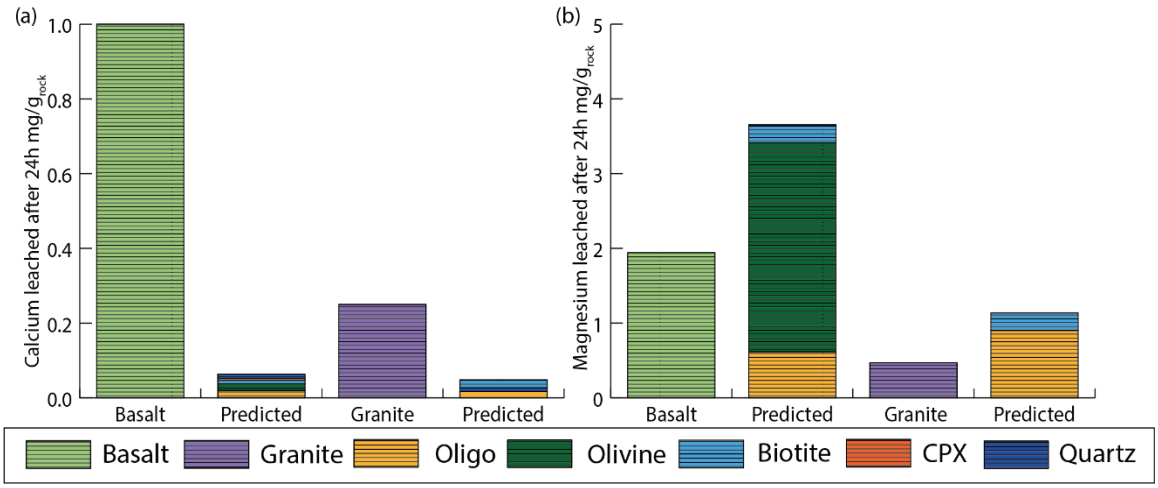

Fig. S3. Concentration, in mg of element leached per g of rock, of (a) calcium and (b) magnesium leached from basalt (green) and granite (purple) compared to the predicted from the equivalent weighted volume of constituent minerals (colors as in Fig.1).

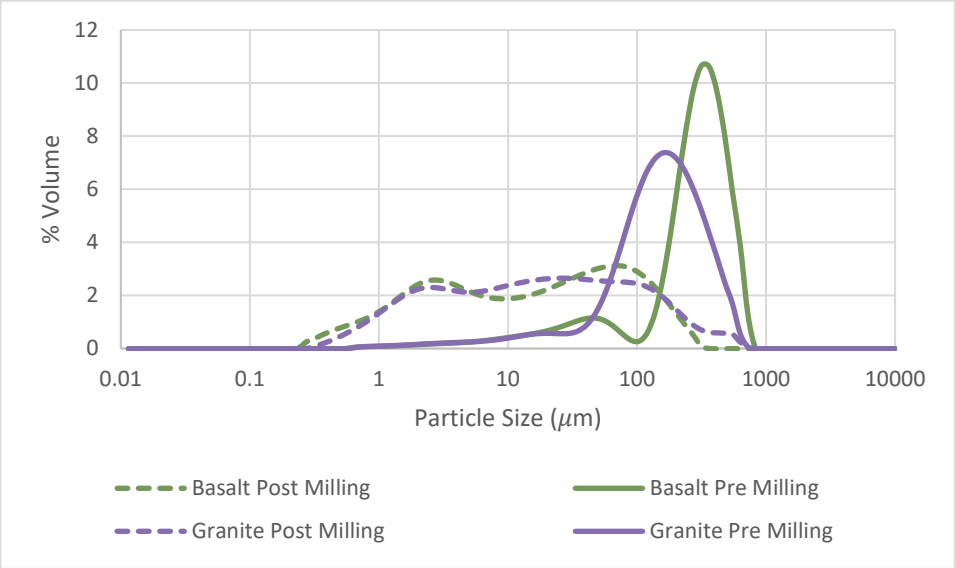

Fig. S4. Particle size distribution by volume of basalt (green) and granite (purple) pre-milling (solid line) and post-milling (dashed line).

Table S1. XRF major oxide analysis of basalt, granite and quartz carried out by ALS Environmental Ltd.

Rock Type	Major Oxide analysis wt%													
	Al_2O_3	BaO	CaO	Cr_2O_3	Fe_2O_3	K_2O	MgO	MnO	Na_2O	P_2O_5	SO_3	SiO_2	SrO	TiO_2	Total
Basalt	14.32	0.08	9.75	0.07	12.27	0.9	10.8	0.17	3.04	0.21	0.05	46.7	0.05	1.38	100.5
Granite	12.51	0.02	0.83	<0.01	2.08	0.88	0.45	0.03	5.87	0.03	0.1	76.86	0.01	0.19	100.4
Quartz	0.09	<0.01	0.03	<0.01	1.06	0.01	0.03	0.01	0.01	<0.01	<0.01	98.97	<0.01	0.02	100.15

Table S2. XRD analysis of mineralogical composition of basalt granite and quartz carried out by ALS Environmental Ltd.

Mineral or mineral group	% Mass		
	Basalt	Granite	Quartz
Clay mineral	1	0	0
Analcime group	8	0	0
Annite - biotite - phlogopite	6	5	0
Muscovite	2	3	0
Clinopyroxene	25	0	0
Orthopyroxene	0	< 1	0
Olivine	17	0	0
Feldspar	39	57	0
Quartz	0	36	100
Ilmenite and/or magnesite	1	0	0
Iron alloy	0	0	< 1

Table S3. BET surface area analysis and surface area change. *Calculated from the difference between the end value and detection limit where the starting surface area is too low for the test to be completed.

Sample Type	Initial/Final	BET Surface Area m2/g	Change in Surface Area m2/g	t-plot Micropore Area m2/g	Change in Micropore Area m2/g
Basalt	Start	0.051	5.417	0.0857	0.5735
	End	5.468		0.6592	
Granite	Start	0.229	7.821	0.0525	0.7499
	End	8.050		0.8024	
Orthoclase	Start	0.167	3.753	0.0217	0.5198
	End	3.920		0.5415	
Oligoclase	Start	0.249	3.191	0.0330	0.6052
	End	3.440		0.6382	
Olivine	Start	0.152	2.298	0.0367	0.2899
	End	2.450		0.3266	
Biotite	Start	<0.05	5.610*	<0.001	0.2200*
	End	5.660		0.2210	
Clinopyroxene	Start	0.549	2.271	0.0337	0.3437
	End	2.820		0.3774	
Quartz	Start	0.106	11.146	0.1240	1.1432
	End	11.252		1.2672	

Table S4. Carbon analysis on minerals and rocks mechanochemically activated in CO_2 and Air (control) before and after leaching in $mgCO_2/g$. The CO_2 leached is then calculated as total CO_2 trapped minus the CO_2 remaining on the solid.

Rock/Mineral	CO_2 in rock $mgCO_2/g$ (Detection limit 0.1 $mgCO_2/g$)											
	control before Leaching			control after leaching			CO_2 before leaching			CO_2 after leaching		
	Replicate 1	Replicate 2	Av	Replicate 1	Replicate 2	Av	Replicate 1	Replicate 2	Av	Replicate 1	Replicate 2	Av
Basalt	2.2	2.2	2.2	1.8	1.8	1.8	15.3	15.6	15.5	15.6	14.7	15.2
Granite	1.1	1.1	1.1	0.7	0.7	0.7	13.8	14.0	13.9	12.9	13.9	13.4
Quartz	<0.1	<0.1	<0.1	<0.1	<0.1	<0.1	1.1	1.0	1.1	1.1	1.0	1.1
Orthoclase	<0.1	<0.1	<0.1	<0.1	<0.1	<0.1	<0.1	<0.1	<0.1	<0.1	<0.1	<0.1
Oligoclase	0.7	0.7	0.7	0.4	0.3	0.4	2.2	1.8	2.0	2.2	1.8	2.0
Olivine	0.4	0.4	0.4	0.4	0.4	0.4	9.5	9.2	9.4	0.7	0.7	0.7
Biotite	2.2	1.9	2.1	1.1	1.1	1.1	9.2	8.9	9.1	3.7	3.7	3.7
Clinopyroxene	<0.1	<0.1	<0.1	<0.1	<0.1	<0.1	1.8	1.8	1.8	1.1	1.1	1.1

Table S5 Leaching experiments measuring the carbon retained within the rock over a 24-hour period (water:rock ratio of 1:10). Each time point was conducted as a separate leaching experiment, and each experiment had a replicate, i.e. for each time point there is Sample 1 and 2 each conducted in a separate centrifuge tube. From each of the centrifuge tubes (Sample 1 and 2) two aliquots of rock powder were selected for carbon analysis (aliquots a and b).
.

			Carbon concentration $mgCO_2/g$			
	Rock:Water	Time	Sample 1		Sample 2	
Rock Type	Ratio (m:m)	hours	a	b	a	b
Granite	1:10	0	13.81	13.88	14.16	13.82
		1	13.30	12.98	12.89	13.15
		2	13.41	13.29	13.33	13.54
		4	13.72	13.27	13.37	13.67
		12	13.38	13.34	13.50	13.35
		24	12.99	12.91	14.36	13.46
Basalt	1:10	0	14.85	15.66	15.40	15.73
		1	15.78	14.71	14.74	15.14
		2	15.50	15.15	14.68	15.05
		4	15.04	14.40	15.45	15.14
		12	14.81	14.72	14.51	14.95
		24	16.20	14.95	14.77	14.58

Table S6 Leaching results after 24 hours using a rock:water ratio of 1:100 and measuring the carbon retained within the rock after leaching for the granite and basalt samples. Samples 1 and 2 are replicate experiments in separate centrifuge tubes. From each of the centrifuge tubes (Samples 1 and 2) two aliquots of rock powder were selected for carbon analysis (aliquots a and b).

Rock Type	Rock:Water Ratio (m:m)	Time hours	Carbon concentration $mgCO_2/g$			
			Sample 1		Sample 2	
			a	b	a	b
Granite	1:100	24	11.26	11.02	13.24	13.17
Basalt	1:100	24	14.22	14.27	14.73	14.82

Table S7. Experimental replicates and average concentration of calcium and magnesium leached from all rocks and minerals after 24h leaching experiments.

Rock/Mineral type	Reactant gas	Ca mg/g			Mg mg/g		
		Replicate 1	Replicate 2	Average	Replicate 1	Replicate 2	Average
Basalt	Control	0.141	0.185	0.163	0.113	0.141	0.127
Basalt	CO2	1.031	0.977	1.004	1.971	1.815	1.893
Granite	Control	0.082	0.058	0.07	0.055	0.041	0.048
Granite	CO2	0.268	0.234	0.251	0.478	0.418	0.448
Quartz	Control	0.033	0.037	0.035	0.015	0.017	0.016
Quartz	CO2	0.061	0.057	0.059	0.022	0.020	0.021
Orthoclase	Control	0.019	0.017	0.018	0.008	0.009	0.008
Orthoclase	CO2	0.023	0.025	0.024	0.004	0.005	0.004
Oligoclase	Control	0.010	0.010	0.01	0.114	0.110	0.112
Oligoclase	CO2	0.012	0.012	0.012	1.546	1.616	1.581
Olivine	Control	0.054	0.057	0.055	1.035	1.077	1.056
Olivine	CO2	0.098	0.094	0.096	16.562	16.332	16.447
Biotite	Control	0.034	0.038	0.036	0.138	0.158	0.148
Biotite	CO2	0.123	0.108	0.115	3.024	2.854	2.939
Clinopyroxene	Control	0.021	0.023	0.022	0.013	0.019	0.016
Clinopyroxene	CO2	0.016	0.021	0.018	0.011	0.009	0.01
Quantification limit		0.0005	0.0005	0.0005	0.0005	0.0005	0.0005